OPERATIONAL PREDICTION SYSTEM NOTES

A Markov Model Approach for Statistical Tropical Cyclone Wind Radii Baseline Forecasts

JOHN A. KNAFF,[a] CHARLES R. SAMPSON,[b] CHRISTOPHER J. SLOCUM,[a] AND NATALIE D. TOURVILLE[c]

[a] *NOAA/Center for Satellite Applications and Research, Fort Collins, Colorado*
[b] *Naval Research Laboratory, Monterey, California*
[c] *Cooperative Institute for Research in the Atmosphere, Colorado State University, Fort Collins, Colorado*

(Manuscript received 26 April 2024, in final form 16 August 2024, accepted 5 September 2024)

ABSTRACT: A skill baseline for 5-day, 34-, 50-, and 64-kt (1 kt = 0.514 m s^{-1}) tropical cyclone (TC) wind radii forecasts is described. The Markov Model Cliper (MMCL) generates a sequence of 12-h forecasts out to a forecast length limited only by the length of the forecast track and intensity. The model employs a climatology of TC size based on infrared satellite imagery, a Markov chain, and a basin-specific drift. MMCL uses the initial wind radii and initial track and intensity forecast as input. Unlike the previously developed wind radii climatology and persistence model (DRCL) that reverts to a climatological size and shape after approximately 48 h, MMCL retains more of its initial size and asymmetry and is likely more palatable for use in operational forecasting. MMCL runs operationally in the western North Pacific basin, the north Indian Ocean, and the Southern Hemisphere for the Joint Typhoon Warning Center (JTWC) in Pearl Harbor, Hawaii. This work also describes the development of Atlantic and eastern North Pacific versions of MMCL. MMCL's formulation allows unlimited extension of forecast lead time without reverting to a generic climatological size and shape. Independent forecast comparisons between MMCL and DRCL for the 2020–22 seasons demonstrates that MMCL's mean absolute errors are generally smaller and biases are closer to zero in North Atlantic and eastern North Pacific basins and in the Southern Hemisphere. This validation includes a few example forecasts and demonstrates that MMCL can be used both as a baseline for assessing wind radii forecast skill and operational use.

SIGNIFICANCE STATEMENT: Skill baselines for forecasts play a key role in assessing the difficulties of individual forecasts and the forecast skill of more complex algorithms. Baselines serve as guidance when better-performing algorithms are unavailable or inconsistent with the operational forecasts. Here, we present a simple and always available algorithm for generating tropical cyclone (TC) wind radii that retain size and shape throughout the forecast better than the prior developed method. The algorithm also better captures the nearly ubiquitous wind field expansion through a tropical cyclone lifetime. This algorithm, developed to use the same initial data as its predecessor, provides more realistic forecast wind radii and has performance that is slightly superior to its predecessor.

KEYWORDS: Tropical cyclones; Wind; Operational forecasting; Statistical forecasting

1. Introduction and motivation

At U.S. tropical cyclone (TC) warning centers, advisories and forecasts provide estimates of the extent of a tropical cyclone's wind field in terms of the maximum extent of wind exceeding the key threshold magnitudes of 34, 50, and 64 kt (1 kt ≈ 0.51 m s^{-1}). These metrics are collectively referred to as "wind radii" and are provided in northeast, southeast, southwest, and northwest geographic quadrants in units of nautical miles (n mi, 1 n mi = 1.852 km) along with forecasts of the maximum sustained 1-min wind or intensity, storm motion, and storm location.

To help forecast and provide a skill baseline for forecasting wind radii, Knaff et al. (2007) developed a set of basin-specific 5-day statistical models in 2004. These models made use of the combination of climatology and persistence of initial conditions, commonly referred to as "CLIPER" models. CLIPER models have a long history of providing skill baselines for TC forecasting parameters (e.g., Neumann 1972; Jarvinen and Neumann 1979; Merrill 1980; Chu 1994; Aberson 1998; Knaff et al. 2003). Knaff et al. (2007) describe the wind radii CLIPER models for the North Atlantic, eastern North Pacific, and western North Pacific basins, which use the moniker "DRCL" in the Automated Tropical Cyclone Forecasting System (ATCF; Sampson and Schrader 2000) database at the National Hurricane Center (NHC), Central Pacific Hurricane Center (CPHC), and the Joint Typhoon Warning Center (JTWC). Henceforth, we will refer to the suite of wind radii CLIPER models as DRCL. The original DRCL basin-specific models (Knaff et al. 2007) were developed using wind radii contained in the advisories 1988–2003 and west of 55°W in the North Atlantic and 2001–03 in the eastern and western North Pacific. Knaff et al. (2018) updated the coefficients of the western North Pacific DRCL model using higher-quality postseason analyzed wind radii (2014–15) described in Sampson et al. (2017, 2018), which resulted in an improved and larger climatology in that basin.

Corresponding author: John Knaff, john.knaff@noaa.gov

DOI: 10.1175/WAF-D-24-0078.1

The climatological vortices developed in Knaff et al. (2007, 2018) employ a storm-motion relative modified Rankine vortex [(1a), (1b)], where the modified Rankine vortex parameters x, a, r_m, and θ_o are functions of the current intensity V_m, storm latitude φ, and translation speed c, and where azimuth θ is measured counterclockwise, starting from the direction 90° to the right of the storm-motion vector in the Northern Hemisphere. Because of the single radial decay term x in (1b), a bias correction that reduces the size of the 64-kt wind radii and increases the 34-kt wind radii is applied. Based on the observations, the persistence of initial wind radii is estimated to have an e-folding time of 32 h. In application, the initial wind radii and parameter x were set a $t = 0$, and at each time the climatological vortex is calculated along the forecast track using the forecast intensity, motion, and location. As the forecast lead time increases, the model becomes increasingly determined by the climatological vortex terms. By 120 h, only 2.3% of the initial conditions remain in the forecast of the TC vortex. Even for forecasts at 48 h, the wind radii forecasts are ~78% climatological vortex:

$$V(r,\ \theta) = (V_m - a)\left(\frac{r}{R_m}\right) + a\cos(\theta - \theta_o),\ r < R_m, \qquad (1a)$$

$$V(r,\ \theta) = (V_m - a)\left(\frac{R_m}{r}\right)^x + a\cos(\theta - \theta_o),\ r \geq R_m. \qquad (1b)$$

Despite the model's reliance on climatology at long leads, it has become a forecast baseline model for wind radii forecasts at the U.S. operational TC forecast centers. The model's formulation is also used in the Monte Carlo TC wind speed probability algorithm (DeMaria et al. 2009, 2013) used at all the operational centers. In general, DRCL performs well in capturing the size and wind radii changes that occur in most TC cases and can be a rather difficult baseline to improve upon until now.

One glaring exception is that the DRCL model struggles with TCs that are initially much smaller or much larger than their climatological counterparts. In nature, the majority of TCs remain in the same size category observed at formation (Lee et al. 2010) and tend to grow throughout their lifetimes (Kossin et al. 2007). Thus, the least operationally useful DRCL forecasts occur when the initial storm is much larger than climatology. In these cases, the DRCL forecast size shrinks to approximate climatology, whether that is expected in the operational forecast or not. Such poor forecasts are rare but result in loss of operational trust in the algorithm. One such case—a dramatic case—was that of Hurricane Sandy (2012) late in its development, when the storm was forecast to hit the east coast of the United States. Figure 1 shows the official and DRCL 34-kt wind radii forecasts for Sandy valid at 1800 UTC 26 October along with the resulting best track values of wind radii. Note that the initial conditions for DRCL are the same as for the official forecast, but that the DRCL 34-kt wind radii shrink as the forecast time increases. Meanwhile, the official forecast in Fig. 1a (and best

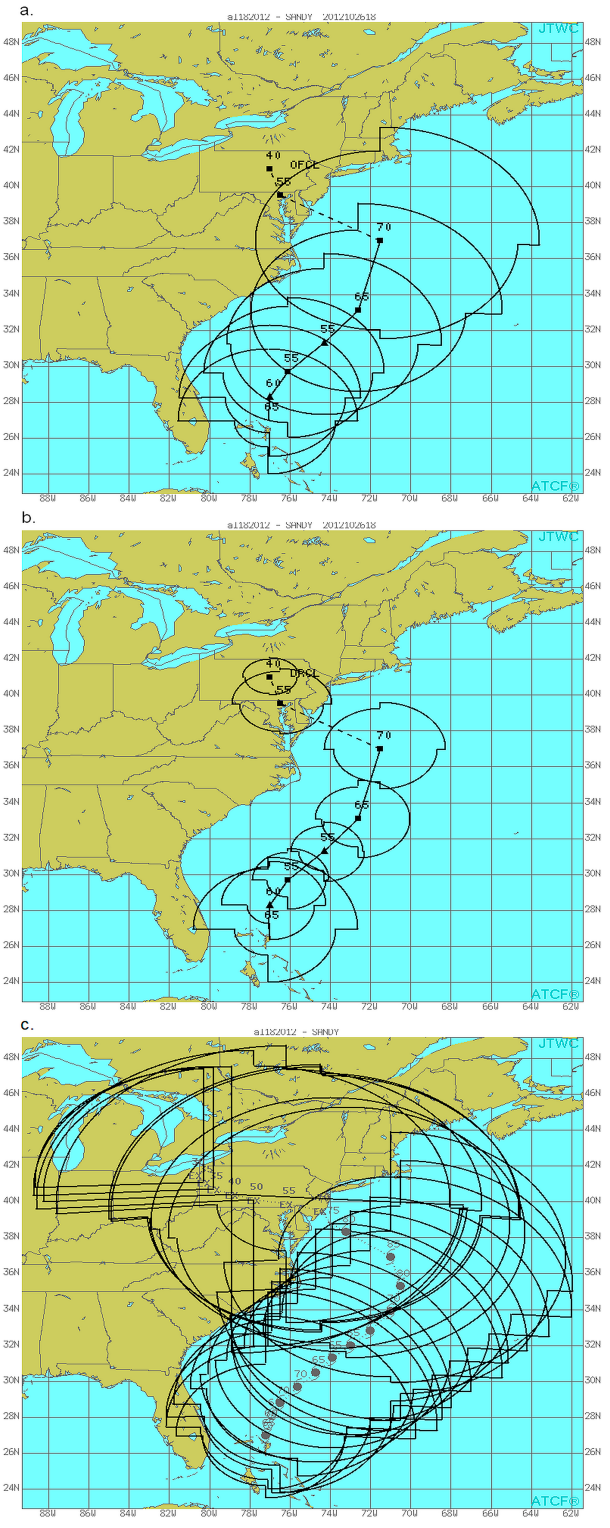

FIG. 1. The 34-kt wind radii forecasts for Hurricane Sandy valid at 1800 UTC 26 Oct 2012 from (a) the NHC official forecast and (b) the DRCL forecast along with the (c) best track intensities and wind radii.

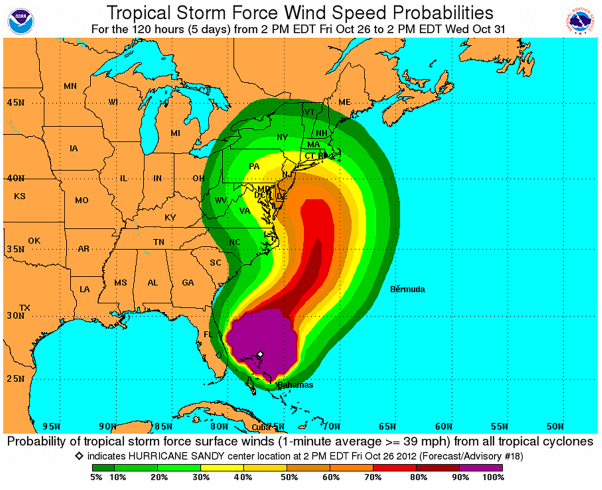

FIG. 2. Cumulative 34-kt wind speed probabilities generated from the 1800 UTC 26 Oct 2012 initial conditions and 2100 UTC official forecasts of track and intensity for Hurricane Sandy. These are available from graphic archives at https://www.nhc.noaa.gov/.

track Fig. 1c) expands the wind radii through the forecast, which makes the DRCL shrinkage at odds with the official forecast and best track expansions. Figure 2 shows the operational 120-h cumulative 34-kt wind speed probabilities initialized at the same time, and the effects of the DRCL wind radii shrinkage can be seen in that product as the forecast wind radii from NHC are nearly as large as the entire cumulative 34-kt wind speed probability swath. One solution to the DRCL issues with extreme sizes and asymmetries is to construct the solution in short increments of 12 h (e.g., a Markov chain), which can possibly retain both the size and asymmetry of the current TC analysis.

This work creates a statistical wind radii prediction model based on a second-order Markov process of TC size, which includes initial conditions that describes the current TC characteristics (storm latitude, storm intensity, 12-h intensity change, zonal translation speed, and meridional translation speed), which are chained together from the initial time to the end of the forecast period. The TC size information comes from a homogeneous record of satellite-based size estimates described in Knaff et al. (2014). This model, MMCL, has been developed for the North Atlantic (AL), eastern North Pacific (EP), western North Pacific (WP), north Indian Ocean (IO), and Southern Hemisphere (SH) basins. It has been in JTWC's operations since late 2020. The IO model is not evaluated in this work due to sample size, but its development is discussed. In the following sections, we describe the data and methods, model development, and results based on independent forecasts from 2020 to 2022. Finally, we will provide a summary and discussion of future work on this topic.

2. Data and methods

a. Developmental data

The TC size record used for MMCL development comes from an infrared (IR) satellite-based method described in Knaff et al. (2014). The IR imagery comes from an archive of TC-centered IR images maintained at the NOAA Center for Satellite Applications and Research (STAR) and the NOAA Cooperative Institute for Research in the Atmosphere (CIRA) at the Colorado State University. These IR images (with central wavelengths near 11 μm) are collected from operational geostationary satellites. The digital imagery is remapped to a Mercator projection with 4-km resolution. Most of the images in the archive are 640 × 480 pixels and centered on the TCs, and the temporal sampling depends on the satellite scan strategy, data availability/quality, and storm location but in general is typically hourly to half hourly. More information on the imagery archive can be found in Knaff et al. (2016, 2018).

The IR-based TC size estimates the radius of 5-kt tangential winds at 850 hPa (R5 in Knaff et al. 2014), which is an approximation of the theoretical radius of zero tangential wind based on storm latitude and the first two 1D principle components of the azimuthal profiles of brightness temperature. Three-hourly R5 estimates provide an extensive homogeneous record of TC size. Even though the intensity is not explicitly used to calculate R5 in the database, R5 is found to increase with intensity (Knaff et al. 2014) and that dependence is removed by creating "fraction TC size" or fR5 as described in Knaff et al. (2017). This fR5 size metric from the IR records used here varies from about 30% to 200% with near Gaussian distribution so the smallest storms and the largest storms range from roughly a third to twice the intensity-based climatology. Later, we will also exploit relationships that provide azimuthally averaged wind radii from R5 and storm intensity described in Knaff et al. (2016).

We also use the TC best tracks for information on TC motion, location, and intensity. The ATCF-formatted best tracks used are constructed by the NHC, CPHC, and JTWC. This same information is converted and disseminated in other formats: The North Atlantic and eastern North Pacific best tracks are in the Hurricane database (HURDAT2; Landsea and Franklin 2013) and both JTWC and NHC best track databases end up in the International Best Track Archive for Climate Stewardship (IBTrACS; Knapp et al. 2010).

Best track intensity, motion, and latitude are interpolated to the 3-hourly records of fR5 at 0000, 0300, 0600, …, 2100 UTC using cubic splines. Then, the 12-h differences of fR5, position, and intensity from $t = -12$ are calculated at the time periods from the 3-hourly record. This forms the dataset for developing a 12-h statistical forecast model based on a second-order Markov process. The dependent variable is 12-h change of fR5 valid at $t = 12$ h, and the independent variables are sine of latitude [$\sin(|\varphi|)$], intensity V_m, the past 12-h change in intensity dV_m, fR5, the past 12-h change in fR5 dfR5, zonal translation speed u, and meridional translation speed v.

b. Statistical model formulation

Using the developmental data discussed above, multiple linear regression is used to form a prediction of the fR5 at $t = 12$ h. As with most skill baselines, the cases are separated into individual basins. The number of cases found in the IO,

TABLE 1. Regression coefficients for 12-h forecasts of *d*fR5 in IO, WP, EP, AL, and SH basins. Boldface indicates statistical significance at the 95th percentile level.

Variable	IO	WP	EP	AL	SH
$\sin(\lvert\varphi\rvert)$	**0.227 09**	**0.297 31**	**0.179 52**	**0.357 22**	**0.252 12**
V_m	0.000 02	**0.000 23**	**0.000 08**	**0.000 36**	0.000 28
dV_m	0.000 12	**−0.000 72**	**−0.000 61**	**−0.001 16**	**−0.000 35**
fR5	**0.899 61**	**0.880 49**	**0.889 02**	**0.823 59**	**0.887 35**
*d*fR5	**−0.320 46**	**−0.271 94**	**−0.264 56**	**−0.247 62**	**−0.210 48**
u	**−0.001 74**	**0.001 72**	0.000 09	**0.001 11**	0.000 68
v	**0.002 54**	**0.002 33**	**0.000 98**	**0.005 18**	**−0.000 45**

WP, EP, AL, and SH basins are 2563, 18 046, 24 352, 21 676, and 14 659, respectively. Because of the large number of cases used, the variables are mostly significant at the 95th percentile using the Student's t test. The notable exceptions are associated with variables V_m and dV_m in the IO, V_m in the SH, and u in the EP and SH. These coefficients are very small but are left in the equations to standardize the 12-h forecast routines. Table 1 provides regression coefficients for the five basins. The dominant terms in all basins are the $\sin(\lvert\varphi\rvert)$, fR5, and *d*fR5 terms, while the other terms have minimal impact on the 12-h forecasts. The coefficients for $\sin(\lvert\varphi\rvert)$, fR5, and *d*fR5 are generally on the order of 10^{-1}, 1, and 10^{-1}, respectively, and suggest that persistence and poleward motion act to expand the radii while observed changes in TC size (*d*fR5) act to contract the radii.

c. Chaining the Markov processes

Up to this point, we have discussed how 12-h forecasts of fR5 are initialized and created, but to create a longer forecast, we must chain successive 12-h forecasts together. To do so, we use the forecast track and intensity to provide initial conditions every 12 h. The procedure is as follows: At $t = 0$, a 12-h forecast of fR5 is made. Then, the 12-h forecast values of $\sin(\lvert\varphi\rvert)$, V_m, dV_m, u, and v are used along with the newly computed fR5 (at 12 h) and *d*fR5 (12-h change in fR5 from $t = 0$ to $t = 12$ h) from the Markov model's first forecast. This process continues until fR5 is forecast all the forecast times, which is typically from 12 to 120 h. Note that extending the forecast time only requires additional forecast track and intensity estimates at these longer forecast lengths. At each forecast time, V_m, latitude, storm speed, and storm direction are retained to allow estimation of R5 and wind radii based on R5 as described in the following subsections.

d. Treatment of initial conditions

Initial wind radii are used in two ways in this model. The first is to estimate the TC size parameters, and the second is to apply the initial wind radii asymmetries as they were observed. In this way, the model always starts with the observed conditions, if they exist.

The TC size parameters R5 and fR5 are calculated from the observed 34-kt wind using the methods described in Knaff et al. (2016). To review, the average of all nonzero 34-kt wind radii $\mathrm{R34_{nza}}$ is calculated. Then, R5 is calculated using $\mathrm{R34_{nza}}$ and the observed V_m in (2). Then, fR5 is calculated using both (3) and (4), where $\mathrm{R5}_c$ is the climatological R5:

$$\mathrm{R5} = (\mathrm{R34_{nza}} + 58.5 - 0.71 \times V_m)/9.26, \tag{2}$$

$$\mathrm{fR5} = \frac{\mathrm{R5}}{\mathrm{R5}_c(V_m)}, \tag{3}$$

$$\mathrm{R5}_c = 7.653 + \left(\frac{V_m}{11.651}\right) - \left(\frac{V_m}{59.067}\right)^2. \tag{4}$$

If all of the 34-kt wind radii quadrants have zero values, which typically happens when V_m is less than 35 kt, $\mathrm{R5} = \mathrm{R5}_c$ and $\mathrm{fR5} = 1$. An identical procedure is done to estimate R5 and fR5 at $t = -12$ h so that the short-term trend in fR5 can be calculated. Finally, if estimates of fR5 at $t = -12$ h do not exist, *d*fR5 is also assigned a value of zero.

Initial wind radii asymmetries are also assigned from the observations at $t = 0$ h. Beyond the initial time, the asymmetries are also blended with the model's wind radii. This process will be described in detail below.

e. The vortex model and wind radii estimation

The vortex model follows from Knaff et al. (2016) and is briefly described here, where azimuthally averaged wind radii are estimated from the V_m and R5 values in (5), and the RMW R_m is provided by an empirical formula (6). Apart from the initial time, described above, V_m and R5 are provided by forecasted values. At all other times, V_m comes from the official forecast and R5 is provided by the Markov process:

$$\begin{pmatrix} \overline{\mathrm{R34}} \\ \overline{\mathrm{R50}} \\ \overline{\mathrm{R64}} \end{pmatrix} = \begin{pmatrix} 0.71V_m + 9.26\mathrm{R5} - 58.5 \\ 0.50V_m + 5.90\mathrm{R5} - 54.1 \\ 0.29V_m + 3.30\mathrm{R5} - 32.9 \end{pmatrix}, \tag{5}$$

$$R_m = 218.3784 - 1.2014V_m + \left(\frac{V_m}{10.9844}\right)^2 - \left(\frac{V_m}{35.3052}\right)^3 - 145.5090\cos(\varphi). \tag{6}$$

To estimate the 2D wind field, a modified Rankine vortex [see (1a), (1b)] is used for each wind radii threshold calculation, i.e., 34, 50, and 64 kt, where the official forecast provides storm motion and θ, V_m, and φ information. The shape parameter x is estimated for each wind radii threshold using the

azimuthally averaged wind radii, and R_m is estimated algebraically as described in Knaff et al. (2015, 2016). The values of the asymmetry a and differential rotation θ_o, on the other hand, are provided by (7) and (8) for the AL basin, respectively, which come from the DRCL model as described in Knaff et al. (2007, see Table 1). Similar equations exist for a and θ_o in the EP basin (Knaff et al. 2007) and WP basin (Knaff et al. 2018). Equations (7) and (8) are also used for the SH basin but modified to account for a negative Coriolis term. The geographic quadrants can be sampled from (1b), and wind radii at the three thresholds can be estimated:

$$a = 1.06 + 0.28c - 0.0026c^2 - 0.08(\varphi - 25) \text{ (AL basin)}, \quad (7)$$

$$\theta_o = 17.0 + 0.08(\varphi - 25) - 1.05c \text{ (AL basin)}. \quad (8)$$

If initial wind radii were available, asymmetric errors are calculated from the differences between modeled and observed wind radii in each quadrant. These are treated as initial errors in each observed wind radius. At the initial time ($t = 0$), the asymmetric wind radii errors are added back to the predicted values so that the observed wind radii equal the predicted wind radii at that time. This ensures that the initial wind radii asymmetries are preserved. At future times, an e-folding time of 32 h (Knaff et al. 2007) is used to blend these initial asymmetric errors throughout all the forecast leads. In the case when a storm is predicted to intensify and wind surpasses a higher wind radii threshold, the initial errors from the next smaller wind radii threshold are used to estimate the asymmetries of these higher wind radii threshold value. For instance, the initial R34 asymmetries for a storm that has maximum winds of 55 kt and values for R50 at $t = 0$ are used to adjust the predicted R64 for that same storm when the maximum winds exceed 64 kt.

f. Growth correction

The 12-h TC size changes in MMCL predictions can be thought of as the residuals of a naïve or persistence forecast (Elsner et al. 2008). Thus, each TC size time series becomes stationary. Or stated differently, the time series exhibits no trend with constant variance and autocorrelation structures over time (Wilks 2011). That is, by using 12-h differencing, the tendency of TCs to grow during their lifetime is removed. This growth tendency of TCs, as observed, is somewhat ubiquitous and has been related to warm air advection and vertical wind shear, extratropical transition and eyewall replacement cycles, importation of angular momentum, and prior interaction with land (Maclay et al. 2008; Chan and Chan 2013; Knaff et al. 2014, 2017), but complete understanding of TC growth over time is still in need of investigation. Growth in R5 has also been observed to be different in different basins (Knaff et al. 2014), and those trends are removed by our Markov process assumption.

To mitigate the removal of TC growth in our algorithm, we add the growth back in using a constant that can be added to each 12-h forecast. This constant is sometimes referred to as a "drift" in the case of random walk models. The years 2017–19 were used to determine the drift in each basin primarily because of the availability of higher quality and reanalyzed wind radii from JTWC (Sampson et al. 2017, 2018; Knaff et al. 2021). Table 2 shows the model drift values for each basin, which are constants added to the predicted value of fR5 at each 12-h step. These constants imply that the growth of TCs measured by fR5 is at a rate of 3.4%, 9.8%, 4.9%, 6.6%, and 8.8% every 12 h in the IO, WP, EP, AL, and SH TC basins, respectively.

TABLE 2. Drift values for each basin determined from the 2017 to 2019 best track values of gale force winds. Values are applied every 12 h to the predicted value of fR5.

IO	WP	EP	AL	SH
0.0336	0.0984	0.0492	0.0656	0.0876

3. Independent validation and example forecasts

In this section, we show the validation of MMCL and DRCL for independent forecasts made during 2020–22 in WP, SH, EP, and AL. The validation is based on finalized wind radii best tracks from JTWC and NHC. The verification strategy follows Knaff and Sampson (2015) so that if any of the quadrants in the best track have nonzero wind radii, all quadrants for that case are verified. This strategy allows the individual quadrant statistics to be combined to form a single measurement of mean absolute error (MAE) and bias (i.e., the mean error) for each forecast lead time. Table 3 provides the number of quadrants verified for 34-, 50-, and 64-kt wind radii (R34, R50, and R64, respectively) at each forecast lead time for each basin. Even with a 3-yr sample, the number of cases available at longer leads and higher wind radii thresholds is relatively small. Short-duration TCs are most evident in the SH and EP, and this fact should be considered when interpreting MAE and bias. Since the verification uses four quadrants per verifying forecast point, 1200 points is the equivalent of 300 individual cases, and many researchers consider 300 cases as a minimum for stable statistics in TC verification. However, many R50 and R64 cases often have fewer than four nonzero quadrants. 900 and 600 may be closer to the number of points that indicate stable statistics. These breakpoints are indicated by boldface in Table 3. These guidelines are likely conservative given the autoregressive nature of MMCL where later forecasts depend on earlier ones. By this measure, the WP and AL R34, R50, and R64 statistics are reasonably stable to 96 h. This is not true for R50 and R64 in the EP and SH where the sample sizes are smaller.

The MAEs of the WP, SH, EP, and AL validation samples are shown in Fig. 3. The MAEs in the WP shown in Fig. 3a suggest that the MAEs associated with MMCL forecasts for all wind radii are nearly always smaller than those of DRCL. This is also true for the SH (Fig. 3b), EP (Fig. 3c), and AL (Fig. 3d). The largest MMCL versus DRCL MAE differences occur in the EP R34 forecasts and the R64 forecasts in all basins. The former is likely due to the better prediction of

TABLE 3. The number of homogeneous quadrants used in the independent validation of wind radii forecasts made in 2020–22 for DRCL and MMCL stratified by basin and lead time. The number of MMCL quadrants is shown in italics. Boldface indicates where we feel the statistics are most stable.

Forecast time (h)	0	12	24	36	48	60	72	96	120
				WP					
R34	**3817**	**3690**	**3481**	**2092**	**2691**	**2335**	**2024**	**1479**	1025
	3817	***3716***	***3497***	***3108***	***2703***	***2342***	***2040***	***1482***	*1029*
R50	**2271**	**2162**	**2072**	**2019**	**1875**	**1655**	**1464**	**1042**	681
	2271	***2191***	***2120***	***2039***	***1886***	***1678***	***1466***	***1052***	*689*
R64	**1535**	**1458**	**1377**	**1309**	**1273**	**1173**	**1070**	**768**	514
	1535	***1439***	***1371***	***1291***	***1254***	***1166***	***1062***	***762***	*511*
				SH					
R34	**3173**	**2840**	**2451**	**2073**	**1758**	**1485**	**1226**	819	544
	3173	***2885***	***2484***	***2084***	***1755***	***1492***	***1237***	*828*	*548*
R50	**1599**	**1421**	**1341**	**1169**	**957**	750	613	405	272
	1599	***1477***	***1391***	***1205***	***994***	*785*	*621*	*418*	*278*
R64	**892**	**785**	**741**	**659**	576	455	393	241	157
	892	***781***	***738***	***644***	*565*	*453*	*380*	*234*	*154*
				EP					
R34	**2419**	**2307**	**2116**	**1828**	**1564**	**1303**	1072	726	451
	2419	***2250***	***2070***	***1798***	***1538***	***1281***	*1057*	*715*	*447*
R50	**1253**	**1216**	**1189**	**1127**	**1017**	868	715	422	227
	1253	***1170***	***1169***	***1111***	***993***	*861*	*697*	*407*	*210*
R64	**776**	**760**	**745**	**716**	670	567	414	221	68
	776	***639***	***615***	*597*	*552*	*445*	*332*	*168*	*56*
				AL					
R34	**3067**	**2834**	**2645**	**2403**	**2153**	**1897**	**1661**	**1258**	905
	3067	***2880***	***2678***	***2430***	***2164***	***1906***	***1671***	***1267***	*908*
R50	**1780**	**1661**	**1554**	**1481**	**1367**	**1253**	**1118**	864	640
	1780	***1666***	***1583***	***1503***	***1382***	***1258***	***1129***	*873*	*651*
R64	**1086**	**1017**	**959**	**915**	**873**	**845**	**782**	**615**	446
	1086	***991***	***949***	***916***	***868***	***837***	***772***	***605***	*443*

smaller storms that occur in this basin (Chavas et al. 2016, and references therein) and their smaller observed growth (Table 2 above). The latter is the result of an improved satellite-based R64 determination [(5)]. Similarly, smaller improvements are also noted for R50 due to an improved R50 formulation. In terms of errors, MMCL produces generally smaller errors for all wind radii.

MAEs, however, are only half the story, a wind radii forecast system could produce smaller MAE by being generally smaller and more symmetric given our verification strategy. To further examine the MMCL versus DRCL comparison, biases from these same samples are shown in Fig. 4. One of the primary goals of this work was to reduce biases caused by the return to climatology that is a fundamental behavior of DRCL. Figure 4 shows that in general this goal has been accomplished. Large improvements in R34 biases are seen in MMCL relative to DRCL in the SH (Fig. 4b), EP (Fig. 4c), and AL (Fig. 4d). In both the SH and AL, large DRCL negative biases are replaced by smaller MMCL high biases. In the EP, MMCL biases are generally smaller for all times and radii. In the WP, R34 biases for MMCL are slightly higher than for DRCL, but the errors (Fig. 3a) are comparable or slightly smaller. The WP DRCL was recently updated with more data, so this is expected. High biases in R50 in DRCL are noticeably reduced in WP (Fig. 4a) and EP (Fig. 4c), whereas initial biases are reduced at short forecast times and increase slightly in SH (Fig. 4b), again noting that the numbers of cases at long leads in the SH are less representative of the initial sample. And R50 biases in the AL (Fig. 4d) are largely unchanged. With respect to R64, in all basins, MMCL reduces biases closer to zero.

These results are encouraging, but does MMCL produce climatological average circles like DRCL at the longer forecast periods? To examine this, we present specific 120-h forecasts that are representative of TC forecasts for each basin.

The first case examined is Hurricane Larry (AL122021) initialized at 1200 UTC 6 September 2021. At this time, Larry was a 105-kt hurricane located in a favorable environment and was forecast to increase 5 kt in intensity in the next 12 h following an eyewall replacement cycle, remained a major hurricane through 48 h, and weakened thereafter as it was forecast to move steadily northwest and recurve after 72 h. The storm was expected to approach, but not strike, eastern Canada and had a typical size with gales extending to 150 n mi in the northeast and southeast quadrants. In the end, Larry made landfall in Newfoundland with maximum winds of 70 kt and a forward speed of 40 kt (Brown 2021). Figure 5a shows the 6-hourly best track from 1200 UTC 6 September to

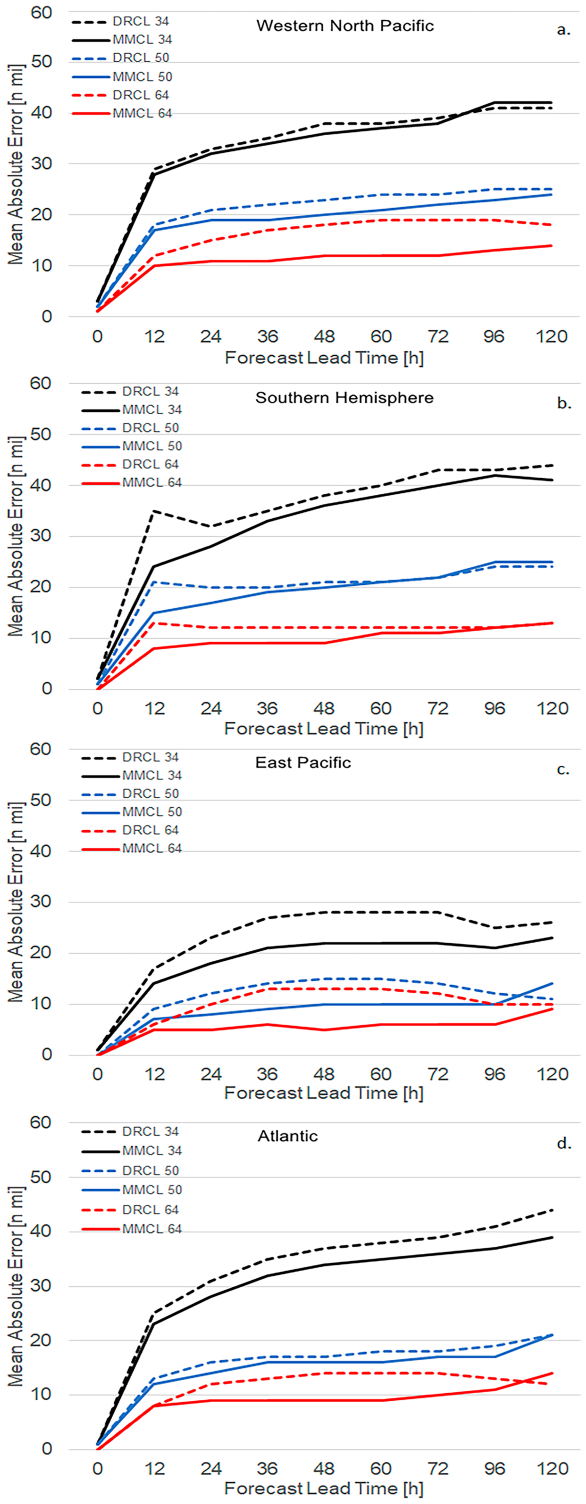

FIG. 3. The 2020–22 homogeneous wind radii MAEs from independent forecasts from DRCL (dashed) and MMCL (solid) for R34 (black), R50 (blue), and R64 (red) in (a) WP, (b) SH, (c) EP, and (d) AL. The number of cases is provided in Table 3.

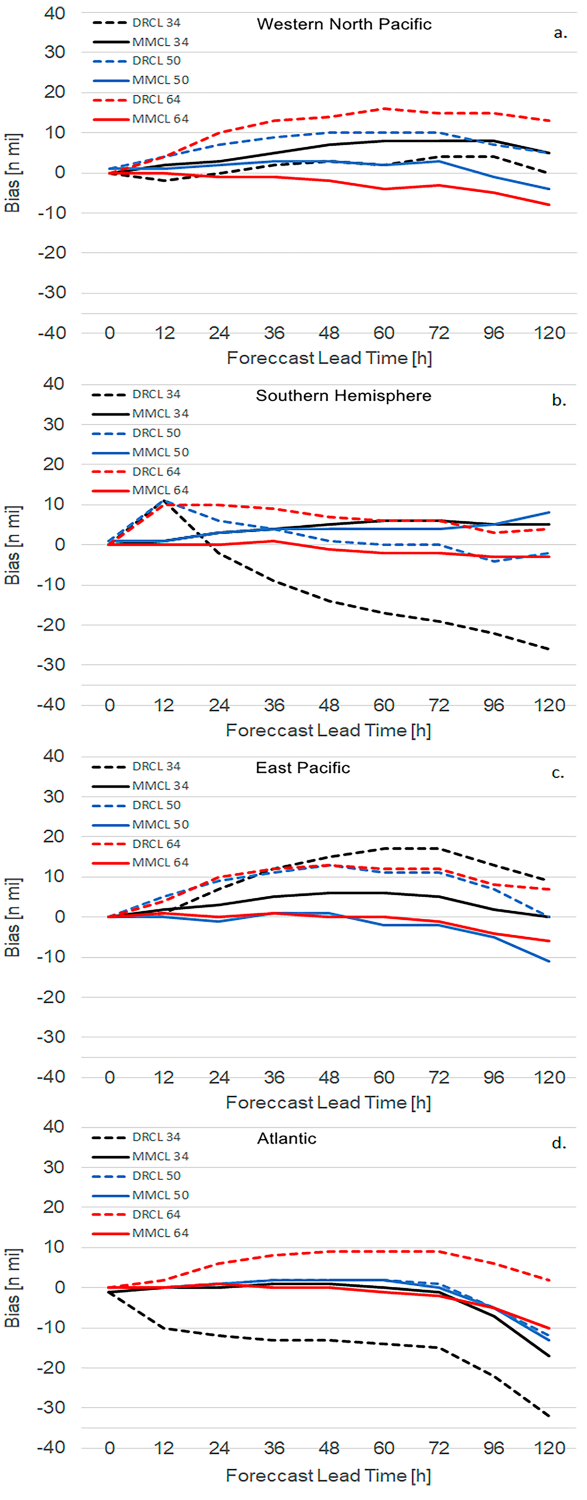

FIG. 4. As in Fig. 3, but for biases.

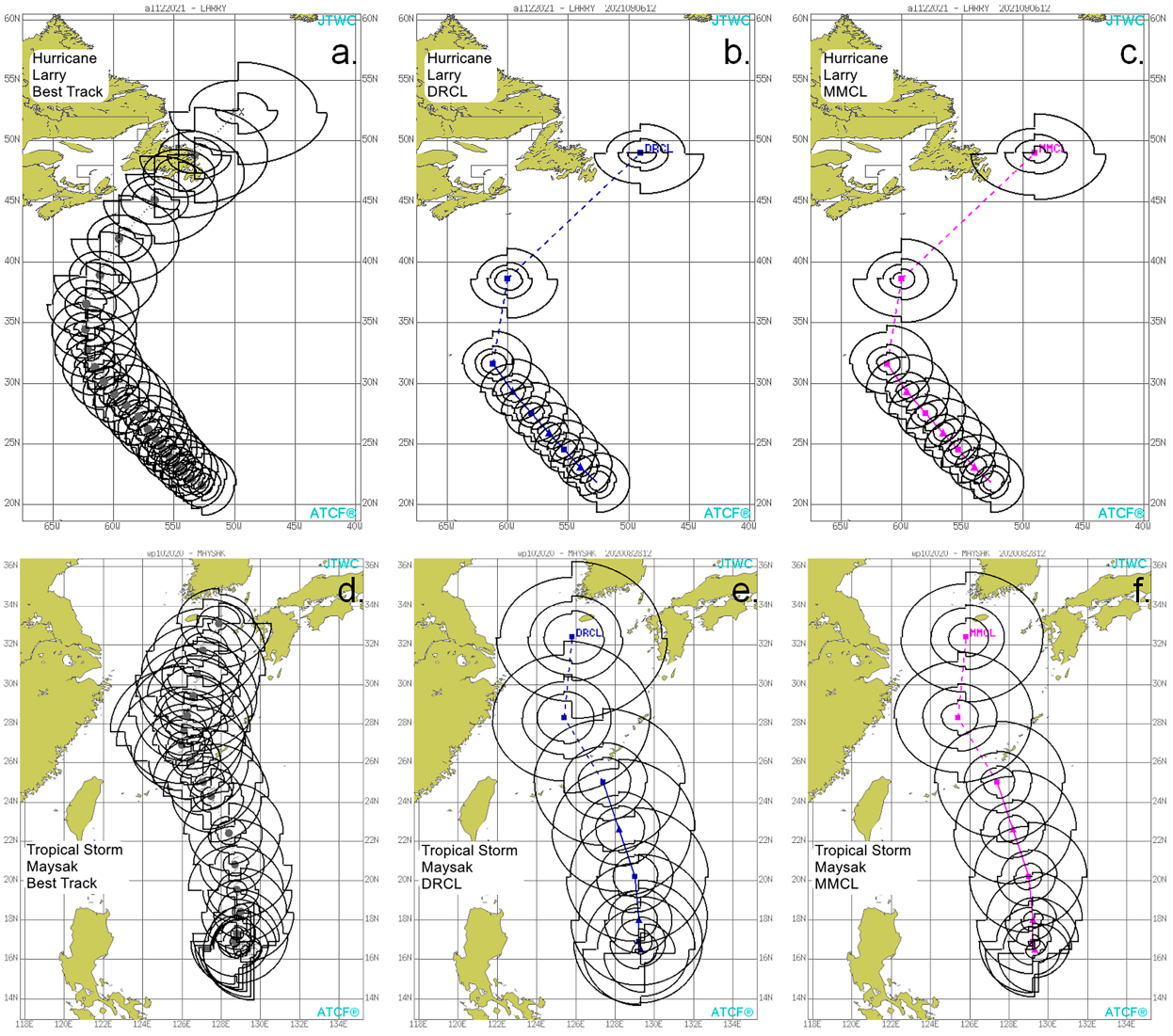

FIG. 5. The black polygons show R34, R50, and R64 moving inward from the outermost polygon. The best track information is shown for every 6 h, and the DRCL and MMCL forecasts are shown at 0, 12, 24, 36, 48, 60, 72, 96, and 120 h. DRCL and MMCL forecasts are independent of their developmental data. Depictions of the 5-day (a) best track, (b) DRCL forecasts, and (c) MMCL forecasts for Hurricane Larry (AL122021) initialized at 1200 UTC 6 Sep 2021 and (d) 5-day best track, (e) DRCL forecasts, and (f) MMCL forecasts for Tropical Storm Maysak (WP102020) initialized at 1200 UTC 28 Aug 2020.

1200 UTC 11 September. The DRCL forecast is shown in Fig. 5b, and the forecast shows only very slight growth of the wind radii except at 96 and 120 h, reflecting a scenario very close to climatology. On the other hand, the MMCL forecast (Fig. 5c) shows pronounced growth after initialization and ultimately a larger storm beyond 48 h. Also note that MMCL forecasts have smaller R64 than DRCL through 4 days, and that these are closer to the best track values. So, in this case, MMCL, by not returning to a climatological solution, made a better forecast.

The second case shown is Tropical Storm Maysak (WP102020) initialized at 1200 UTC 28 August 2020 with a 35-kt intensity; Maysak was then forecast to intensify to 70 kt in 24 h and to 110 kt by 72 h. It was also expected to move nearly due north, affecting smaller Japanese islands, Kyushu, and South Korea—a very important forecast for JTWC. At initialization, Maysak was large and asymmetric with gales extending 90, 30, 120, and 40 n mi in the northeast, southeast, southwest, and northwest quadrants, respectively. The 5-day best track depicts the storm symmetrizing over the next few days, with little indication of an increase in size, but eventually growing larger off the coast of South Korea (Fig. 5d). The JTWC intensity forecast (input into both DRCL and MMCL) indicated a more rapid attainment of 110 kt than was observed, then a weaker storm at days 3–5. In this scenario, DRCL (Fig. 5e) predicts a large typhoon, one that is typical of the new climatology (Knaff et al. 2018) and continued growth of the gales through 5 days. MMCL (Fig. 5f), on the other hand, forecasts a smaller

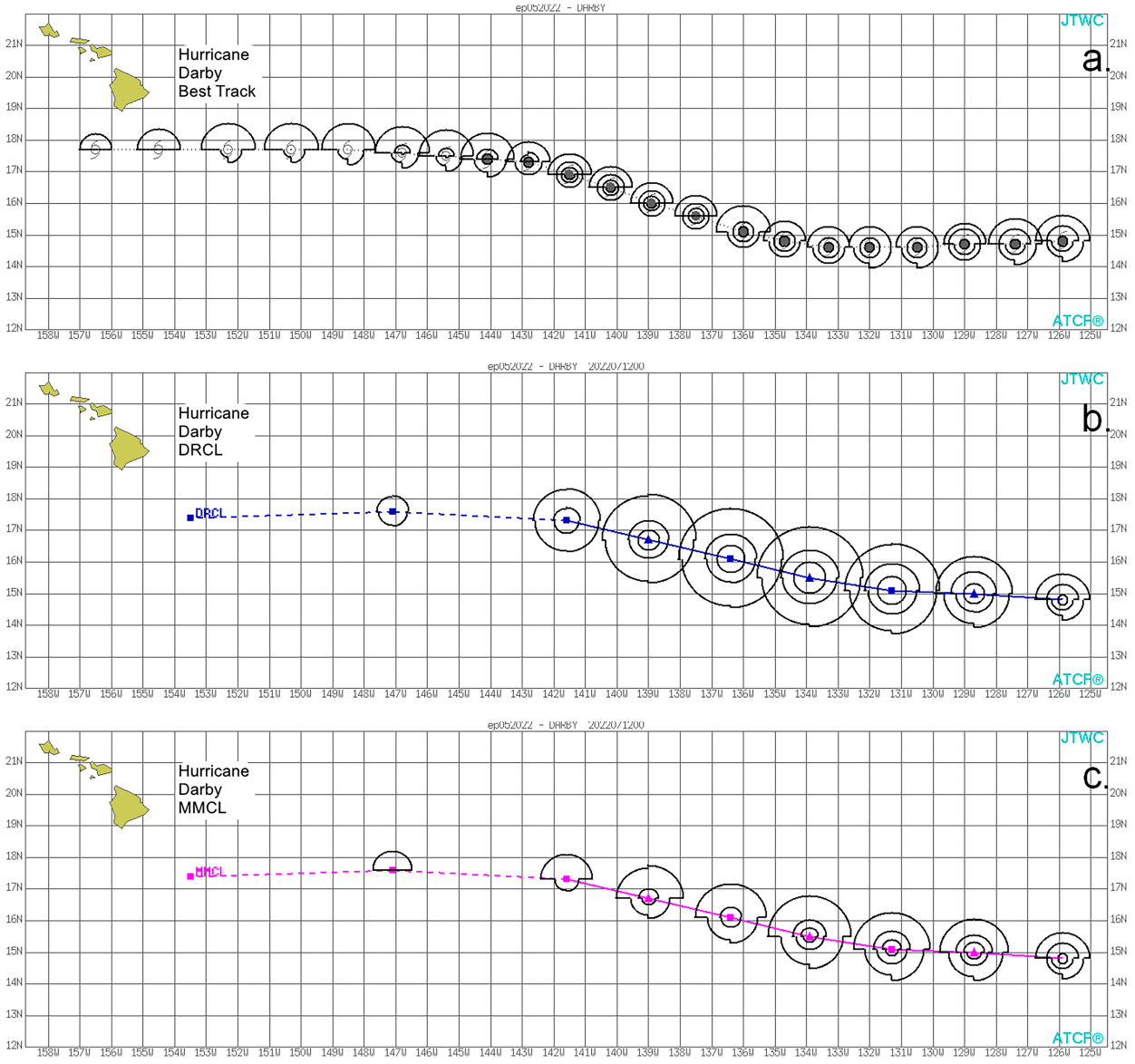

FIG. 6. As in Fig. 5, except that depictions are of the 5-day (a) best track, (b) DRCL forecasts, and (c) MMCL forecasts for Hurricane Darby (EP052022) initialized at 1200 UTC 12 Jul 2022.

and more realistic evolution as Maysak intensified rapidly by indicating slower growth during intensification. The MMCL forecast also produced much smaller R50 and R64 forecasts, which were much closer to those depicted in the best track. Here again, MMCL produced a smaller and more realistic forecast when the TC was intensifying. This was expected as the dV_m term is negative in Table 1 and acts to slow growth during intensification.

The final case shown is a forecast for Hurricane Darby (EP052022) initialized at 1200 UTC 12 July 2022 with a 115-kt intensity and very small wind radii (R34 $\leq$ 40 n mi, R64 = 10 n mi). The TC was expected to move slightly north of due west with steady and then more rapid weakening with the possibility of a very weak TC affecting the Hawaiian Islands. The best track (Fig. 6a), however, indicates that the storm moved slightly south of west weakened for 18 h, then intensified to 100 kt at 1800 UTC 13 July 2022 where it remained for 6 h, and then began to weaken (Bucci 2021). During this time, the wind radii became slightly smaller. The differences between the best track and forecasts affected both DRCL (Fig. 6b) and MMCL (Fig. 6c), but in different ways. As DRCL relaxed to a larger climatology, MMCL grew much slower. The higher anticipated latitude resulted in larger wind radii forecasts in both, but the forecast of weakening, also resulted in larger wind radii in MMCL. Here, however, the largest errors are associated with DRCL's tendency to approach a climatological mean at longer forecast lengths. MMCL, free of this constraint, produced more realistic wind radii.

R50 and R64 forecasts remained much smaller in Darby until the vortex weakened to a tropical storm. MMCL produces more realistic and better-performing forecasts than DRCL for Darby because MMCL uses separate R5-based estimates of R34, R50, and R64 in (5), which is unlike DRCL, and creates more realistic and smaller R50 and R64 forecasts. Figure 5 also shows similar improvements in MMCL R50 and R64 forecasts in Hurricane Larry and Tropical Storm Maysak. These results are consistent with the improved biases shown in Fig. 4.

The summary statistics and case studies presented above indicate that the MMCL baseline is in most cases a superior performing and more realistic baseline forecast of wind radii. With that information in mind, we now provide a short summary and discussion.

4. Summary, discussion, and future work

This paper discusses the development of a skill baseline tropical cyclone wind radii method, MMCL, that addresses a known shortcoming of the more traditional climatology- and persistence-based DRCL. DRCL's persistence component is rather short-lived, and the model returns to a climatological vortex following about 48 h. In nature, TC wind fields tend to grow, although at different rates in different basins (Table 2). Large storms rarely shrink to a climatological size for any time other than during their decay. In extremely large TCs, the DRCL forecast wind radii are generally too small, while in extremely small TCs, the DRCL forecast wind radii are generally too big. Examples of these effects are shown in the extremely large Hurricane Sandy (2012) case in Fig. 1, and more typical cases are provided in Figs. 5 and 6.

The solution developed here uses a satellite record of TC size to develop a 12-h forecast of TC size change based on current and routinely available information and developing a Markov chain of 12-h forecasts along any intensity and track forecast of any length. As part of the development, a climatological drift for each basin is also added to each 12-h forecast to account for tendency for TCs to grow as a function of time. Thus, MMCL provides a more realistic baseline forecast based on information provided from the initial conditions and the official forecast and that does not revert to a climatological size.

Results based on 3 years of independent forecasts suggest that this model produces forecasts with generally smaller MAEs and improved biases for all wind radii thresholds. The largest MAE improvements of MMCL compared with DRCL are found in the EP and AL basins; however, biases are most improved in the SH, EP, and AL basins, particularly for R34 and R64.

MMCL is in the operational forecast guidance suite at JTWC for TCs occurring in the WP, IO, and SH basins and can produce forecasts in the AL and EP. While its performance represents only a small improvement in wind radii forecast baseline capability, it addresses known shortcomings of DRCL with extremely large or extremely small TCs that persist beyond 2 days.

MMCL forecasts, while simple and representing a baseline, may aid in the operational wind radii consensus forecasts (RVCN; Sampson and Knaff 2015) or replace the DRCL member in the consensus. It is particularly useful for longer leads where DRCL reverts to climatology. It also has realistic forecasts for inclusion in RVCN, particularly since it provides stability in the forecast when NWP model forecast intensities decay and their radii drop out of the RVCN consensus. Both DRCL and MMCL can be easily extended to longer forecast lead times, but whereas in DRCL longer-lead forecasts would just reflect the static climatology of TC size, MMCL produces wind radii forecasts that are physically consistent with the official forecast information and with the initial conditions. Thus, as official forecasts improve, MMCL will also likely improve. With that in mind, the MMCL formulation and similar strategies could be applied to synthetic tracks created to assess wind risks for real-time forecasts (e.g., in wind radii realizations for the operational wind speed probabilities; DeMaria et al. 2013) or even insurance risks and climate change scenarios. Finally, MMCL provides a more realistic baseline for verification of wind radii forecasts, one that can be easily extended for forecasts beyond 5 days.

Acknowledgments. This work was accomplished while the authors were employed by the NOAA Center for Satellite Applications and Research to support several tropical cyclone applications and at the Naval Research Laboratory, Monterey, California, supported by ONR Award N0001420WX00517 to NRL Monterey and the NOAA Cooperative Institute for Research in the Atmosphere at Colorado State University (NOAA Grant NA17RJ1228). We also thank Chris Landsea and the other anonymous reviewer for their careful and constructive review of the manuscript. The scientific results and conclusions, as well as any views or opinions expressed herein, are those of the authors and do not necessarily reflect those of the NOAA or the Department of Commerce.

Data availability statement. This publication uses data from geostationary satellites contained in the STAR/CIRA tropical cyclone IR image archive. Those data, which are in a non-standard format and reduced bit precision, are available upon request. Alternatively, raw IR data are available from NOAA CLASS (https://www.avl.class.noaa.gov/saa/products/welcome), Multi-Format Client-Agnostic File Extraction Through Contextual HTTP (MCFETCH; https://mcfetch.ssec.wisc.edu/), and EUMETSAT (https://www.eumetsat.int/access-our-data). We also make use of tropical cyclone best tracks available that are openly available from JTWC (https://www.metoc.navy.mil/jtwc/jtwc.html?best-tracks), the National Hurricane Center, and the Central Pacific Hurricane Center (https://ftp.nhc.noaa.gov/atcf/).

REFERENCES

Aberson, S. D., 1998: Five-day tropical cyclone track forecasts in the North Atlantic basin. *Wea. Forecasting*, **13**, 1005–1015, https://doi.org/10.1175/1520-0434(1998)013<1005:FDTCTF>2.0.CO;2.

Brown, D. P., 2021: Tropical cyclone report: Hurricane Larry (AL122021), 31 August–11 September 2021. NOAA NWS NHC Tech Rep., 34 pp., https://www.nhc.noaa.gov/data/tcr/AL122021_Larry.pdf.

Bucci, L., 2021: Tropical cyclone report: Hurricane Darby (EP052022), 9–17 July 2022. NOAA NWS NHC Tech Rep., 16 pp., https://www.nhc.noaa.gov/data/tcr/EP052022_Darby.pdf.

Chan, K. T. F., and J. C. L. Chan, 2013: Angular momentum transports and synoptic flow patterns associated with tropical cyclone size change. *Mon. Wea. Rev.*, **141**, 3985–4007, https://doi.org/10.1175/MWR-D-12-00204.1.

Chavas, D. R., N. Lin, W. Dong, and Y. Lin, 2016: Observed tropical cyclone size revisited. *J. Climate*, **29**, 2923–2939, https://doi.org/10.1175/JCLI-D-15-0731.1.

Chu, J.-H., 1994: A regression model for the western North Pacific tropical cyclone intensity forecasts. NRL Memo. Rep. 7541-94-7215, 33 pp.

DeMaria, M., J. A. Knaff, R. D. Knabb, C. Lauer, C. R. Sampson, and R. T. DeMaria, 2009: A new method for estimating tropical cyclone wind speed probabilities. *Wea. Forecasting*, **24**, 1573–1591, https://doi.org/10.1175/2009WAF2222286.1.

——, and Coauthors, 2013: Improvements to the operational tropical cyclone wind speed probability model. *Wea. Forecasting*, **28**, 586–602, https://doi.org/10.1175/WAF-D-12-00116.1.

Elsner, J. B., T. H. Jagger, M. Dickinson, and D. Rowe, 2008: Improving multiseason forecasts of North Atlantic hurricane activity. *J. Climate*, **21**, 1209–1219, https://doi.org/10.1175/2007JCLI1731.1.

Jarvinen, B. R., and C. J. Neumann, 1979: Statistical forecasts of tropical cyclone intensity for the North Atlantic basin. NOAA Tech. Memo. NWS NHC-10, 24 pp., https://repository.library.noaa.gov/view/noaa/6555.

Knaff, J. A., and C. R. Sampson, 2015: After a decade are Atlantic tropical cyclone gale force wind radii forecasts now skillful? *Wea. Forecasting*, **30**, 702–709, https://doi.org/10.1175/WAF-D-14-00149.1.

——, M. DeMaria, C. R. Sampson, and J. M. Gross, 2003: Statistical, 5-day tropical cyclone intensity forecasts derived from climatology and persistence. *Wea. Forecasting*, **18**, 80–92, https://doi.org/10.1175/1520-0434(2003)018<0080:SDTCIF>2.0.CO;2.

——, C. R. Sampson, M. DeMaria, T. P. Marchok, J. M. Gross, and C. J. McAdie, 2007: Statistical tropical cyclone wind radii prediction using climatology and persistence. *Wea. Forecasting*, **22**, 781–791, https://doi.org/10.1175/WAF1026.1.

——, S. P. Longmore, and D. A. Molenar, 2014: An objective satellite-based tropical cyclone size climatology. *J. Climate*, **27**, 455–476, https://doi.org/10.1175/JCLI-D-13-00096.1.

——, ——, R. T. DeMaria, and D. A. Molenar, 2015: Improved tropical-cyclone flight-level wind estimates using routine infrared satellite reconnaissance. *J. Appl. Meteor. Climatol.*, **54**, 463–478, https://doi.org/10.1175/JAMC-D-14-0112.1.

——, C. J. Slocum, K. D. Musgrave, C. R. Sampson, and B. R. Strahl, 2016: Using routinely available information to estimate tropical cyclone wind structure. *Mon. Wea. Rev.*, **144**, 1233–1247, https://doi.org/10.1175/MWR-D-15-0267.1.

——, C. R. Sampson, and G. Chirokova, 2017: A global statistical–dynamical tropical cyclone wind radii forecast scheme. *Wea. Forecasting*, **32**, 629–644, https://doi.org/10.1175/WAF-D-16-0168.1.

——, ——, and K. D. Musgrave, 2018: Statistical tropical cyclone wind radii prediction using climatology and persistence: Updates for the western North Pacific. *Wea. Forecasting*, **33**, 1093–1098, https://doi.org/10.1175/WAF-D-18-0027.1.

——, and Coauthors, 2021: Estimating tropical cyclone surface winds: Current status, emerging technologies, historical evolution, and a look to the future. *Trop. Cyclone Res. Rev.*, **10**, 125–150, https://doi.org/10.1016/j.tcrr.2021.09.002.

Knapp, K. R., M. C. Kruk, D. H. Levinson, H. J. Diamond, and C. J. Neumann, 2010: The International Best Track Archive for Climate Stewardship (IBTrACS). *Bull. Amer. Meteor. Soc.*, **91**, 363–376, https://doi.org/10.1175/2009BAMS2755.1.

Kossin, J. P., J. A. Knaff, H. I. Berger, D. C. Herndon, T. A. Cram, C. S. Velden, R. J. Murnane, and J. D. Hawkins, 2007: Estimating hurricane wind structure in the absence of aircraft reconnaissance. *Wea. Forecasting*, **22**, 89–101, https://doi.org/10.1175/WAF985.1.

Landsea, C. W., and J. L. Franklin, 2013: Atlantic hurricane database uncertainty and presentation of a new database format. *Mon. Wea. Rev.*, **141**, 3576–3592, https://doi.org/10.1175/MWR-D-12-00254.1.

Lee, C., K. K. W. Cheung, W. Fang, and R. L. Elsberry, 2010: Initial maintenance of tropical cyclone size in the western North Pacific. *Mon. Wea. Rev.*, **138**, 3207–3223, https://doi.org/10.1175/2010MWR3023.1.

Maclay, K. S., M. DeMaria, and T. H. Vonder Haar, 2008: Tropical cyclone inner-core kinetic energy evolution. *Mon. Wea. Rev.*, **136**, 4882–4898, https://doi.org/10.1175/2008MWR2268.1.

Merrill, R. T., 1980: A statistical tropical cyclone motion forecasting system for the Gulf of Mexico. NOAA Tech. Memo. NWS NHC 14, 23 pp., https://repository.library.noaa.gov/view/noaa/7028.

Neumann, C. J., 1972: An alternate to the HURRAN (hurricane analog) tropical cyclone forecast system. NOAA Tech. Memo. NWS SR-62, 28 pp., https://repository.library.noaa.gov/view/noaa/3605.

Sampson, C. R., and A. J. Schrader, 2000: The Automated Tropical Cyclone Forecasting System (Version 3.2). *Bull. Amer. Meteor. Soc.*, **81**, 1231–1240, https://doi.org/10.1175/1520-0477(2000)081<1231:TATCFS>2.3.CO;2.

——, and J. A. Knaff, 2015: A consensus forecast for tropical cyclone gale wind radii. *Wea. Forecasting*, **30**, 1397–1403, https://doi.org/10.1175/WAF-D-15-0009.1.

——, E. M. Fukada, J. A. Knaff, B. R. Strahl, M. J. Brennan, and T. P. Marchok, 2017: Tropical cyclone gale wind radii estimates for the western North Pacific. *Wea. Forecasting*, **32**, 1029–1040, https://doi.org/10.1175/WAF-D-16-0196.1.

——, J. S. Goerss, J. A. Knaff, B. R. Strahl, E. M. Fukada, and E. A. Serra, 2018: Tropical cyclone gale wind radii estimates, forecasts, and error forecasts for the western North Pacific. *Wea. Forecasting*, **33**, 1081–1092, https://doi.org/10.1175/WAF-D-17-0153.1.

Wilks, D. S., 2011: *Statistical Methods in the Atmospheric Sciences*. 3rd ed. Elsevier, 676 pp.